360 *Chem. Mater.* **2010,** *22,* 360–370
DOI:10.1021/cm902748k

CHEMISTRY OF MATERIALS
Article

Dodecanethiol-Stabilized Platinum Nanoparticles Obtained by a Two-Phase Method: Synthesis, Characterization, Mechanism of Formation, and Electrocatalytic Properties

Eryza G. Castro,[†] Rodrigo V. Salvatierra,[†] Wido H. Schreiner,[‡] Marcela M. Oliveira,[†] and Aldo J. G. Zarbin*,[†]

[†]*Departamento de Química, Universidade Federal do Paraná (UFPR), CP 19081, CEP 81531-990, Curitiba-PR-Brazil and* [‡]*Departamento de Física, Universidade Federal do Paraná (UFPR), CP 19081, CEP 81531-990, Curitiba-PR-Brazil*

Received September 3, 2009. Revised Manuscript Received November 25, 2009

Dodecanethiol-stabilized platinum nanoparticles of less than 3 nm have been synthesized for the first time through a modified two-phase liquid−liquid route. The H_2PtCl_6 precursor was transferred from water to toluene using tetra-*n*-octylammonium bromide, followed by the addition of dodecanethiol. Results obtained by Raman spectroscopy, X-ray absorption near edge structure (XANES), and extended X-ray absorption fine structure (EXAFS) indicate a reaction between the platinum precursor and the thiol, resulting in a Pt(II)-stable complex that cannot be reduced by sodium borohydride. The Pt nanoparticles were obtained by the reduction of the platinum precursor before the introduction of dodecanethiol. The time interval at which the dodecanethiol was added to the reaction was used to control the size of the nanoparticles. The formation of dodecanethiol-stabilized Pt nanoparticles with fcc structure and average diameter of 1.7, 2.2 and 2.4 nm was confirmed by Fourier-transform infrared spectroscopy (FT-IR), X-ray diffractometry, transmission electron microscopy, X-ray photoelectron spectroscopy (XPS), XANES, and EXAFS. All of the obtained nanoparticles were electrocatalytically active for methanol oxidation, and the differences in catalytic activity between different samples were related to the size and morphology of the nanoparticles.

Introduction

Nanosized particles of noble metals have attracted much interest in recent years due to their size-dependent properties and potential applications in several areas, such as microelectronics, optoelectronics, catalysis, photocatalysis, magnetic materials, information storage, sensors, etc.[1,2] Platinum nanoparticles, for instance, have been synthesized with efforts aimed at increasing the catalytic surface area relative to the bulk platinum,[3−5] thereby yielding better and more selective catalysts. Pt nanoparticles have been used extensively as efficient catalyst-electrodes in the electrooxidation of alcohols in fuel cell technology.[6−9] Aside from being used as catalysts, Pt nanoparticles have also been produced for use as sensors,[10] electronic devices,[11] fillers and active components in composite materials,[12] and other applications.

Because most physical and chemical properties of these metal nanoparticles (NPs) depend on their size and shape, it is imperative to develop synthetic routes that give nonagglomerated, uniform nanoparticles with a well-controlled mean size and a narrow size distribution. An important feature in the production of the metallic NPs is the ability to keep them physically isolated, thereby preventing irreversible aggregation. The stability of the NPs is commonly achieved using different capping molecules (e.g., alkanethiols) that bind to the NP surface, preventing aggregation and making the NPs soluble in various solvents.[13−18]

*To whom correspondence should be addressed. E-mail: aldo@quimica.ufpr.br.

(1) Marzan, L. M. *Mater. Today* **2004**, 26.
(2) Winnischofer, H.; Rocha, T. C. R.; Nunes, W. C.; Socolovsky, L. M.; Knobel, M.; Zanchet, D. *ACS Nano* **2008**, *2*, 1313.
(3) Siani, A.; Wigal, K. R.; Alexeev, O. S.; Amiridis, M. D. *J. Catal.* **2008**, *257*, 5.
(4) Lin, C.-S.; Khan, M. R.; Lin, S. D. *J. Colloid Interface Sci.* **2006**, *299*, 678.
(5) Yoo, E.; Okata, T.; Akita, T.; Kohyama, M.; Nakamura, J.; Honma, I. *Nano Lett.* **2009**, *9*, 2255.
(6) Tian, N.; Zhou, Z.-Y.; Sun, S.-G.; Ding, Y.; Wang, Z.-L. *Science* **2007**, *316*, 732.
(7) Che, G.; Lakshmi, B. B.; Fisher, E. R.; Charles, R. *Nature* **1988**, *393*, 346.
(8) Sanles-Sobrido, M.; Correa-Duarte; Carregal-Romero, S.; Rodriguez-Gonzalez, B.; Alvarez-Puebla, R. A.; Herves, P.; Liz-Marzan, L. M. *Chem. Mater.* **2009**, *21*, 1531.
(9) Wen, F.; Simon, U. *Chem. Mater.* **2007**, *19*, 3370.
(10) Krasteva, N.; Besnard, I.; Guse, B.; Bauer, R. E.; Mullen, K.; Yasuda, A.; Vossmeyer, T. *Nano Lett.* **2002**, *2*, 551.
(11) Tu, W.; Takai, K.; Fukui, K.; Miyazaki, A.; Enoki, T. *J. Phys. Chem. B* **2003**, *107*, 10134.
(12) Sivakumar, C. *Electrochim. Acta* **2007**, *52*, 4182.
(13) Yang, J.; Lee, J. Y.; Too, H.-P. *Anal. Chim. Acta* **2006**, *571*, 206.
(14) Eklund, S. E.; Cliffel, D. E. *Langmuir* **2004**, *20*, 6012.
(15) Yang, J.; Lee, J. Y.; Deivaraj, T. C.; Too, H.-P. *Langmuir* **2003**, *19*, 10361.
(16) Liu, J.; Sutton, J.; Roberts, C. B. *J. Phys. Chem. C* **2007**, *111*, 11566.
(17) Dablemont, C.; Lang, P.; Mangeney, C.; Piquemal, J.-Y.; Etkov, V.; Herbst, F.; Viau, G. *Langmuir* **2008**, *24*, 5841.
(18) Yee, C.; Scotti, M.; Ulman, A.; White, H.; Rafailovich, M.; Sokolov, J. *Langmuir* **1999**, *15*, 4314.

 Published on Web 12/22/2009

A variety of different approaches have been developed for the preparation of metal NPs, including microemulsion,[19] sonochemical,[20] polyol,[21] template,[22] solvent-reduction,[23] reverse micelle,[24] and ionic liquid[25] methods, among others. Wet synthesis starting from a solution of the NP precursor represents one of the most promising routes to NPs in terms of controlling the synthetic parameters, cost, and potential for high-volume production. Brust et al. developed one of the simplest and most popular synthetic routes to produce thiol-stabilized gold nanoparticles;[26] this method involves phase transfer of $[AuCl_4]^-$ anions from aqueous to organic solution in a two-phase liquid/liquid system, followed by reduction with sodium borohydride in the presence of dodecanethiol.[26] The proposed mechanism indicates that the nucleation and growth of the gold nanoparticles and the surface attachment of the thiol molecules occurs simultaneously in a single step. This preparation method was further adapted for preparing silver NPs.[27]

Although the two-phase route developed by Brust has met with great success in the preparation of thiol-functionalized Au and Ag nanoparticles, there are no reports on the utilization of this route for the preparation of Pt nanoparticles. Some attempts to prepare Pt NPs by the Brust procedure have failed, as described by Eklund and Cliffel,[14] and to the best of our knowledge there are no reports describing the reasons for this failure. Other routes for preparing stable and organic-soluble alkanethiol-stabilized Pt NPs have been developed, such as the one-phase synthetic method described by Yee et al.[18] and the two-phase routes developed by Sarathy et al.,[28,29] Zhao et al.,[30] and Yang et al.,[15] in which freshly prepared Pt nanoparticles (rather than platinum ions) were transferred from the aqueous phase to the organic phase by direct thiolation.

In this work we describe the synthesis, characterization, and study of the electrocatalytic activity of dodecanethiol-stabilized platinum nanoparticles based on the synthetic route developed by Brust. Using characterization techniques as Raman spectroscopy, XANES, and EXAFS, we demonstrate that the formation of a stable complex in the organic phase between the platinum precursor and the thiol molecules avoids reduction of the platinum precursor (and consequently inhibition of NP formation), which probably was responsible for the failure of previous attempts to produce Pt NPs by this route. Also, we demonstrate that stable Pt NPs with controlled size (from 1.7 to 2.4 nm) can be easily obtained by a simple inversion of the sequence in which the thiol and the reducing agent are added to the precursor solution. To the best of our knowledge, this is the first report on the utilization of a modified-Brust route for obtaining stable and size-controlled platinum nanoparticles.

Experimental Section

Analytical grade dihydrogen hexachloroplatinate (IV) hexahydrate (Merck), tetra-*n*-octylammonium bromide (Merck), sodium borohydride (Merck), dodecanethiol (Merck), ethanol (Merck), methanol (Merck), sulfuric acid (Merck), toluene (Merck), and Nafion perfluorinated ion-exchange resin 5 wt % solution (Aldrich) were used as received. Water was deionized using a Milli-Q Ultra-Pure-Water Purification System. Three different experimental setups were employed.

Experiment 1. First, 10 mL of tetra-*n*-octylammonium bromide (TOAB, 0.05 mol L^{-1}, 5.00×10^{-4} mol) in toluene was added slowly (dropwise, 30 drops per minute) to a 125 mL round-bottomed flask containing an aqueous solution of $H_2PtCl_6 \cdot 6H_2O$ (3.75 mL, 0.03 mol L^{-1}, 1.25×10^{-4} mol). After addition of the TOAB solution was complete, the mixture was stirred for 10 min. After this time, 51 μL (2.50×10^{-4} mol) of dodecanethiol (DT) was added with stirring, followed by rapid injection (using a 50 mL syringe) of 3.5 mL of a 0.4 mol L^{-1} aqueous solution of sodium borohydride. No changes in the color of the solutions (both aqueous and organic phases) were detected, nor was the appearance of any insoluble compound. The mixture was stirred for 3 h, and then the organic phase was separated.

Experiment 2. With the aim of identification of the species present in the organic solution, experiment 1 was repeated but without the addition of the reducing agent (sodium borohydride). After the addition of DT, the organic phase was separated with a separation funnel and was characterized using different techniques. Two solutions have been prepared, adding two different amounts of dodecanethiol, 51 μL (2.50×10^{-4} mol) and 102 μL (5.00×10^{-4} mol), resulting in two solutions with Pt/thiol molar ratios of 1:2 and 1:4. To facilitate discussion, these two solutions will be referred to here as **Pt/DT-1/2** and **Pt/DT-1/4**. The mixture was stirred for 3 h, and then the organic phase was separated. The procedure was also repeated without the addition of dodecanethiol, yielding the solution named **Pt/TOAB**.

Experiment 3. This experiment was similar to experiment 1 but involved inverting the order in which DT and sodium borohydride were added to the system. First, 10 mL of tetra-*n*-octylammonium bromide (TOAB, 0.05 mol L^{-1}, 5.00×10^{-4} mol) in toluene was added slowly (dropwise, 30 drops per minute) to a 125-mL round-bottomed flask containing an aqueous solution of $H_2PtCl_6 \cdot 6H_2O$ (3.75 mL, 0.03 mol L^{-1}, 1.25×10^{-4} mol). After addition of the TOAB solution was complete, the mixture was stirred for 10 min. After this time, an aqueous solution of sodium borohydride (3.5 mL, 0.4 mol L^{-1}) was quickly injected into the system using a 50 mL syringe. The pale-yellow organic phase immediately became brown. Next, 51 μL (2.50×10^{-4} mol) of dodecanethiol (DT) was added after specific and well-controlled time intervals from the addition of the borohydride solution. Five samples were

(19) Pal, A.; Shah, S.; Belochapkine, S.; Tanner, D.; Magner, E.; Devi, S. *Colloids Surf., A* **2009**, *337*, 205.
(20) Park, J.; Atobe, M.; Fuchigami, T. *Electrochim. Acta* **2005**, *51*, 848.
(21) Couto, G. G.; Klein, J. J.; Schreiner, W. H.; Mosca, D. H.; Oliveira, A. J. A.; Zarbin, A. J. G. *J. Colloid Interface Sci.* **2007**, *311*, 461.
(22) Sarkar, J.; John, V. T.; He, J.; Brooks, C.; Gandhi, D.; Nunes, A.; Ramanath, G.; Bose, A. *Chem. Mater.* **2008**, *20*, 5301.
(23) Teranishi, T.; Hosoe, M.; Tanaka, T.; Miyake, M. *J. Phys. Chem. B* **1999**, *103*, 3818.
(24) Croy, J. R.; Mostafa, S.; Heinrich, H.; Cuenya, B. R. *Catal. Lett.* **2009**, *131*, 21.
(25) Kim, K.-S.; Demberelnyamba, D.; Lee, H. *Langmuir* **2004**, *20*, 556.
(26) Brust, M.; Walker, M.; Bethell, D.; Schiffrin, D. J.; Whyman, R. J. *Chem. Soc. Chem. Commun.* **1994**, 801.
(27) Oliveira, M. M.; Zanchet, D.; Ugarte, D.; Zarbin, A. J. G. *J. Colloid Interface Sci.* **2005**, *292*, 429.
(28) Sarathy, K. V.; Kulkarni, G. U.; Rao, C. N. R. *Chem. Commun.* **1997**, 537.
(29) Sarathy, K. V.; Raina, G.; Yadav, R. T.; Kulkarni, G. U.; Rao, C. N. R. *J. Phys. Chem. B* **1997**, *101*, 9876.
(30) Zhao, S.-Y.; Chen, S.-H.; Wang, S.-Y.; Li, D.-G.; Ma, H.-Y. *Langmuir* **2002**, *18*, 3315.

prepared by adding the dodecanethiol after 30, 60, 90, 180, and 300 s from the beginning of the introduction of the borohydride solution to the reaction medium. For each sample preparation, the mixture was subsequently stirred for 3 h, followed by separation of the organic phase using a separation funnel. To the organic solution containing the NPs was added 40 mL of ethanol, and the mixture was maintained in a freezer (−18 °C) for 1 h to precipitate the NPs. The NPs were then separated by centrifugation (3000 rpm for 10 min), washed several times with ethanol (to eliminate excess TOAB and DT), redissolved in toluene, and kept under argon atmosphere until use. The Pt NPs obtained in this work will be referred to here as **PtNP-30**, **PtNP-60**, **PtNP-90**, **PtNP-180** and **PtNP-300**, indicating samples in which addition of the dodecanethiol took place after 30, 60, 90, 180, and 300 s from the beginning of the reduction.

UV−vis spectra were collected directly from the NP solution (after the washing step) in a Shimadzu UV-2450 spectrophotometer, using toluene as the reference, in the 190−900 nm range.

X-ray diffraction measurements were done in a Shimadzu XD-3A diffractometer using Cu Kα radiation, with 40 kV and 40 mA, at 0.02° scan rate (in 2θ), with a step of 10 s per point. Powder silicon reflections were used for 2θ calibration. The samples were prepared by dropping the NP toluene solution over the glass sample-holder and waiting for solvent evaporation. This procedure was repeated several times in order to obtain a thick film of the NPs.

Transmission electron microscopy (TEM) was done in a JEOL JEM 120 kV instrument. High-resolution transmission electron microscopy (HRTEM) was performed in a JEOL JEM 3010 microscope operating at 300 KV (1.7 Å resolution). The samples were prepared by dropping the NP solution on standard hole cupper grids covered by a thin film of amorphous carbon. The histograms of the size distribution were obtained by counting 750 NPs from the TEM images for each sample. The data were analyzed by means of the Microcal Origin 5.0 software.

FT-IR spectra of the samples were obtained with a BioRad FTS 3500 GX spectrophotometer in the 4000−400 cm^{-1} range with 32 scans. The samples were prepared by dropping the NP toluene solution over a KBr crystal and waiting for solvent evaporation. Measurements were carried out directly from the KBr crystal.

The Raman spectra were obtained in a Renishaw Raman Image spectrophotometer, coupled to an optical microscope that focuses the incident radiation down to a spot of approximately 1 μm. A He−Ne laser (emitting at 632.8 nm) was used, with an incidence potency of 2 mW over the 2000−200 cm^{-1} range.

Dynamic light scattering (DLS) measurements were carried out using a Nanotrac NAS 35 instrument with the nominal detection beam varying from 0.8 to 6500 nm, using 300 μL of the toluene dispersion of the nanoparticles. Measurements were obtained in three scans of 30 s each.

XPS experiments were performed using a commercial system (VG Microtech ESCA3000 with Mg Kα and Al Kα radiations) with a base pressure of 3×10^{-10} mbar. The spectra were obtained at a takeoff angle of 45° (normal) using a hemispherical energy analyzer with an overall energy resolution of ∼0.8 eV. The binding energy scales were referenced by setting the C_{1s} binding energy to 285.0 eV. The XPS analyses were performed by assuming core level spectra with Gaussian line shapes after standard Shirley background subtraction. Samples were prepared by dispersion on an aluminum sample holder prior to each experiment.

The XAS experiments were performed on the XAS beamline of the National Synchrotron Light Laboratory (LNLS, Brazil). EXAFS and XANES spectra were collected at the platinum L_3 edge (11 564 eV) using a Si (111) monochromator calibrated at the L_3 edge of metallic platinum. Pt foil and an aqueous solution of H_2PtCl_6 (0.03 mol L^{-1}, pH 1.85) were used as reference compounds. The experimental XANES spectra were collected with a resolution of ∼0.3 eV and were background corrected using a Victoreen-fit and normalized in the range of 11 520−11 600 eV. This procedure was achieved using the program Athena. The EXAFS spectra were normalized, analyzed and fitted using the programs WINXAS, Athena, and Artemis. The values of the nearest-neighbor atoms (N) and their distances (R) were obtained from the Pt crystallographic data.

The electrocatalytic activity of the platinum nanoparticles on the methanol oxidation reaction was evaluated by cyclic voltammetry. The voltammograms were performed in a mixture of 1 mol L^{-1} methanol and 0.5 mol L^{-1} H_2SO_4 on a Micro-Autolab potentiostat, in a conventional three electrode one-compartment cell consisting of the working electrode, a platinum wire counter electrode, and an Ag/AgCl reference electrode. The working electrode was a glassy carbon electrode, 3 mm in diameter, coated with the nanoparticles. The Pt nanoparticles were loaded onto the electrode as follows: 1 mg of the nanoparticles was dispersed in 238 μL of a water/isopropanol mixture (1/1 v/v) containing 12 μL of a 0.5 wt % Nafion solution. The mixture was sonicated for 20 min. A 6 μL portion of this mixture was dropped onto the glassy carbon electrode and dried at room temperature for 24 h.

Results and Discussion

The first attempt to prepare the Pt NPs (experiment 1) was carried out following the route described by Brust et al.[26] but substituting the gold precursor $HAuCl_4$ with the platinum precursor H_2PtCl_6. The aqueous-to-toluene transfer of the $[PtCl_6]^{2-}$ ions by the TOAB was evidenced by a color change (colorless to pale yellow) observable in the organic phase after 10 min of stirring in the presence of TOAB. The pale-yellow color of the organic phase became more intense after the addition of dodecanethiol. However, contrary to results found with gold ions, no changes to the system were observed after the addition of sodium borohydride (excess), which means that the sodium borohydride was not able to reduce the platinum ions. This was an unexpected result since the reduction of the $[PtCl_6]^{2-}$ by BH_4^- in the presence of water (yielding metallic platinum, hydrogen, sodium cations and chloride anions) is expected to be favorable ($\Delta E^\circ = +0.175$ V). Initially, we believed that the failure of this reduction was due to formation of a toluene-soluble complex of the platinum precursor and dodecanethiol, which could not be reduced by the borohydride ions. To test this hypothesis, we carried out experiment 2, in which the experimental procedure of experiment 1 was repeated but sodium borohydride was omitted. After transfer of $[PtCl_6]^{2-}$ to the organic phase, the dodecanethiol was added to the system in two different Pt/DT molar amounts, **Pt/DT-1/2** and **Pt/DT-1/4**. A blank solution (without the addition of the DT) was also prepared simply by isolating the organic phase after transferring $[PtCl_6]^{2-}$ (**Pt/TOAB**).

The UV−vis spectrum of the H_2PtCl_6 aqueous solution used in this work (Figure S1 in the Supporting

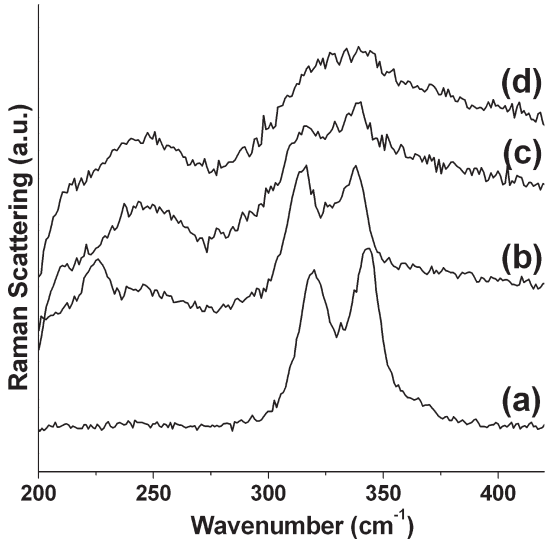

Figure 1. Raman spectra: (a) aqueous solution of $[PtCl_6]^{2-}$, (b) toluene solution of $[PtCl_6]^{2-}$ after the phase transfer (**Pt/TBOA**), (c) toluene solution of $[PtCl_6]^{2-}$ after the addition of dodecanethiol in a Pt/thiol ratio of 1/2 (**Pt/DT-1/2**), and (d) toluene solution of $[PtCl_6]^{2-}$ after the addition of dodecanethiol in a Pt/thiol ratio of 1/4 (**Pt/DT-1/4**).

Information) is characterized by the presence of two chlorine-to-platinum charge transfer bands at 201 and 256 nm and two weak d−d bands at 377 and 456 nm.[31,32] It is well-known that aqueous solutions of H_2PtCl_6 form a mixture of various metal complexes that are in dynamic equilibrium. This mixture forms because the chloro complex can suffer hydrolysis, in which some Cl^- ligands can be replaced by water molecules or OH^- ligands.[33] The exact composition of these solutions depends on several factors, such as pH, concentration, and the presence of other species in solution. Under the experimental conditions employed in this work (pH 1.85 and a concentration of 3.0×10^{-2} mol L^{-1}), the literature reports that the octahedral $[PtCl_6]^{2-}$ complex remains unchanged, although some authors have suggested that one Cl^- can be displaced by H_2O.[33] The spectrum of the solution employed in this work does not show oxygen-to-platinum charge transfer bands, confirming that most of the platinum ions in solution are in the form of hexachloroplatinate. On the basis of this discussion, we believe that the octahedral unit $[PtCl_6]^{2-}$ was, for the most part, unchanged during the aqueous−toluene phase transfer.

Figure 1 shows the Raman spectra of $[PtCl_6]^{2-}$ in an aqueous solution (Figure 1a) and in a toluene solution after the TOAB phase transfer (**Pt/TOAB**, Figure 1b). Figure 1a shows the typical Pt−Cl vibrational bands at 319 and 343 cm^{-1}, which are due to the antisymmetrical and symmetrical Pt−Cl stretching, respectively.[34] No Pt−O vibrational modes were detected in the spectrum. The two Pt−Cl bands remain in the spectrum of the **Pt/TOAB** solution (Figure 1b), showing an increase in

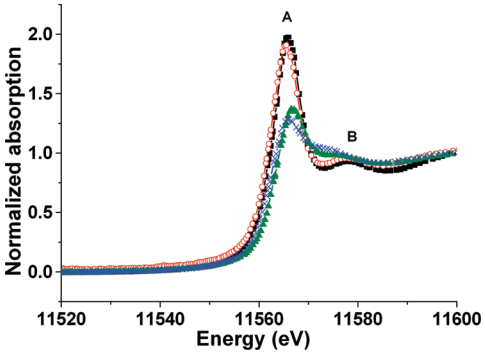

Figure 2. XANES spectra: (black, ■) aqueous solution of $[PtCl_6]^{2-}$, (red, ○) toluene solution of $[PtCl_6]^{2-}$ after the phase transfer (**Pt/TBOA**), (green, ▲) toluene solution of $[PtCl_6]^{2-}$ after the addition of dodecanethiol in a Pt/thiol ratio of 1/2 (**Pt/DT-1/2**), and (blue, ×) toluene solution of $[PtCl_6]^{2-}$ after the addition of dodecanethiol in a Pt/thiol ratio of 1/4 (**Pt/DT-1/4**).

bandwidth and a small shift to lower wavenumber, confirming that the $[PtCl_6]^{2-}$ structure was maintained in both aqueous and toluene solution. However, the exchange of some Cl^- ligands by Br^- (from TOAB), forming $[PtCl_{6-x}Br_x]^{2-}$, cannot be discarded (in fact the slight redshift of the Raman peaks is consistent with the formation of some Pt−Br bonds). After the addition of dodecanethiol, the spectra of the solutions changed, as observable in parts c and d of Figure 1. The intensity of the Pt−Cl stretching bands vanished in the spectrum of **Pt/DT-1/2** (Figure 1c), and in the spectrum of sample **Pt/DT-1/4** the Pt−Cl bands disappeared (Figure 1d). These results could be a strong indication of a ligand-exchange in the platinum coordination shell after dodecanethiol addition.

The toluene solutions of **Pt/TOAB**, **Pt/DT-1/2**, and **Pt/DT-1/4** and the aqueous solution of H_2PtCl_6 were characterized by X-ray absorption spectroscopy (XAS) at the Pt L_3-edge, both in the XANES (X-ray absorption near-edge structure) and EXAFS (extended X-ray absorption fine structure) region. Figure 2 shows the normalized XANES spectra of these samples. The absorption at the Pt L_3 edge at 11 564 eV is associated with the excitation of $2p_{3/2}$ electrons to 5d states,[35] and the absorption hump located approximately 3 eV past the edge (marked A in Figure 2) is commonly called the "white line". The low-intensity absorption at approximately 11 580 eV (marked B in Figure 2) is also characteristic of XANES spectra of platinum. In Pt XANES, the intensity of the white line reflects the electron density of the platinum atoms: the higher the intensity of the white line, the lower the electron density of the platinum atoms (or in other words, the higher the oxidation state of Pt).[36,37] Quantitative determination of the platinum oxidation state by analysis of the white line intensity of the XANES spectrum was reported by Yoshida et al.[36] and Hall et al.[37] According these authors, the XANES spectra of Pt(IV) and Pt(II)

(31) Donald, L.; Swihart, L.; Mason, W. R. *Inorg. Chem.* **1970**, *9*, 1749.
(32) Cox, L. E.; Peters, D. G. *Inorg. Chem.* **1970**, *9*, 1927.
(33) Spieker, W. A.; Liu, J.; Miller, J. T.; Kropf, A. J.; Regalbuto, J. R. *Appl. Catal., A* **2002**, *232*, 219.
(34) Shelimov, B.; Lambert, J.-F.; Che, M.; Didillon, B. *J. Catal.* **1999**, *185*, 462.
(35) Siani, A.; Wigal, K. R.; Alexeev, O. S.; Amiridis, M. D. *J. Catal.* **2008**, *257*, 16.
(36) Yoshida, H.; Nonoyama, S.; Yazawa, N. Y.; Hattori, T. *Phys. Scr.* **2005**, *T115*, 813.
(37) Hall, M. D.; Foran, G. J.; Zhang, M.; Beale, P. J.; Hambley, T. W. *J. Am. Chem. Soc.* **2003**, *125*, 7524.

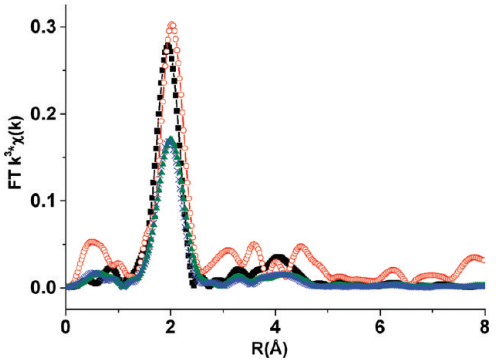

Figure 3. Fourier transformed EXAFS spectra: (black ■) aqueous solution of $[PtCl_6]^{2-}$, (red ○) toluene solution of $[PtCl_6]^{2-}$ after the phase transfer (**Pt/TBOA**), (green ▲) toluene solution of $[PtCl_6]^{2-}$ after the addition of dodecanethiol in a Pt/thiol ratio of 1/2 (**Pt/DT-1/2**), and (blue ×) toluene solution of $[PtCl_6]^{2-}$ after the addition of dodecanethiol in a Pt/thiol ratio of 1/4 (**Pt/DT-1/4**).

differ in the heights of their white lines, independent of the coordination sphere. On the basis of the intensity of the absorbance of peak A relative to the baseline under B (see Figure 2), the authors proposed that the ratio A/B can be used to diagnose the oxidation state of Pt (the highest A/B ratio of 2.51 corresponds to 100% Pt(IV) and the lowest A/B ratio of 1.52 corresponds to 100% Pt(II). Intermediate values were attributed to mixtures of the two oxidation states in different proportions). Figure 2 shows that the spectra of $[PtCl_6]^{2-}$ in both water and toluene solution are similar, corroborating the previous result that the $[PtCl_6]^{2-}$ octahedral structure is maintained after the water−toluene phase-transfer. The A/B ratio observed in these spectra (calculated according to the procedure described in ref 37, see Figure S2 in the Supporting Information) was 2.4, confirming the Pt(IV) oxidation state. A significant reduction in the white line intensity is observed for the toluene solutions of $[PtCl_6]^{2-}$ after addition of dodecanethiol, characterized by A/B ratios of 1.6 and 1.5 for the samples **Pt/DT-1/2** and **Pt/DT-1/4**, respectively. These results indicate a Pt(IV) to Pt(II) reduction caused by the presence of dodecanethiol.

The experimental EXAFS spectra collected from the solutions were fitted and Fourier transformed (k^3, Kaiser window). Figure 3 shows the radial distribution functions obtained after the FT treatment. The fitted structural parameters for the samples are presented in Table 1. The FT profile of the $[PtCl_6]^{2-}$ aqueous solution shows one intense peak due to a Pt coordination sphere consisting of six chlorine ions at a Pt−Cl distance of 2.32 Å.[33,34,38] After the water-to-toluene phase transfer, the spectrum is almost the same, corroborating the previous results in which the chlorine hexacoordination sphere remains unchanged after the phase transfer. However, addition of dodecanethiol causes marked changes in the coordination sphere of the platinum, as can be seen in Figure 3. There is a clear reduction in the amplitude of the FT peak after addition of dodecanethiol, indicating a reduction in the coordination number of platinum. In fact, the fit

Table 1. Structural Parameters Obtained from EXAFS Analysis at the L_3 Edge of Pt

sample	coordination number	R (Å)	σ^2
$[PtCl_6]^{2-}$ (aqueous)	6	2.32	
$[PtCl_6]^{2-}$ (toluene)	6.58	2.32	1.16×10^{-3}
Pt/DT-1/2 (toluene)	3.95	2.34	1.38×10^{-3}
Pt/DT-1/4 (toluene)	3.97	2.34	2.49×10^{-3}
Pt foil	12	2.771	3.68×10^{-3}
PtNP-30	6.72	2.747	6.26×10^{-3}
PtNP-60	7.59	2.758	5.71×10^{-3}
PtNP-90	8.42	2.748	5.45×10^{-3}

structural parameters for both **Pt/DT-1/2** and **Pt/DT-1/4** (Table 1) show platinum coordination numbers of four, as expected for Pt(II)-based square-planar complexes.

The complementary data obtained by UV−vis, Raman, and XAS presented earlier indicate that the $[PtCl_6]^{2-}$ octahedral structure is maintained both in aqueous solution and after transferring the TBOA to toluene. The Pt(IV) ions are reduced to Pt(II) in toluene after dodecanethiol addition, and this reduction is accompanied by a decrease in the platinum coordination number from six to four. Dodecanethiol acts as the reducing agent in this process; this alkanethiol can be oxidized to the disulfide $H_{24}C_{12}-S-S-C_{12}H_{24}$. Several reports have described the oxidation of alkanethiols to the high stable disulfide species.[39] The Pt(IV) to Pt(II) reduction process requires 2 mol of electrons for each mol of $[PtCl_6]^{2-}$. Considering that each mole of dodecanethiol releases 1 mol of electrons to be oxidized to the disulfide, the stoichiometry is exact for producing the sample **Pt/DT-1/2**. In this sample, all of the available thiol is oxidized to the corresponding disulfide, which can act as a bidentate ligand in the Pt(II) square-planar complex. The other two coordination sites are probably occupied by the chloride ions that remain from the original coordination of the $[PtCl_6]^{2-}$. The presence of the chloride ligands in the complex **Pt/DT-1/2** was detected by Raman spectroscopy (Figure 1). In the sample **Pt/DT-1/4**, there are 2 mol of excess dodecanethiol that will not be oxidized. These "free" dodecanethiol molecules can displace the chloride ligands remaining in the **Pt/DT-1/2** sample and occupy the resulting coordination sites. The absence of Pt−Cl bonds in sample **Pt/DT-1/4** was previously detected by Raman spectroscopy (Figure 1). Another possibility is the formation of various complex structures in which the disulfide bridges the two Pt(II) centers or polymeric structures in which two metal centers are linked by a thiol molecule. Some proposals concerning the formation of **Pt/DT-1/2** and **Pt/DT-1/4** are presented in the Supporting Information (Figures S3−S6).

Although the mechanism of formation and the structure of the complex resulting from the addition of dodecanethiol in the toluene solution of $[PtCl_6]^{2-}$ are uncertain at present, there are no doubts that this complex is formed and is highly stable toward sodium borohydride reduction, which precludes the synthesis of Pt NPs via this route. To avoid this obstacle, we proposed a small

(38) Bel'skaya, O. B.; Karymova, R. Kh.; Kochubey, D. I.; Duplayakin, V. K. *Kin. Catal.* **2008**, *49*, 720.

(39) Witt, D. *Synthesis* **2008**, *16*, 2491.

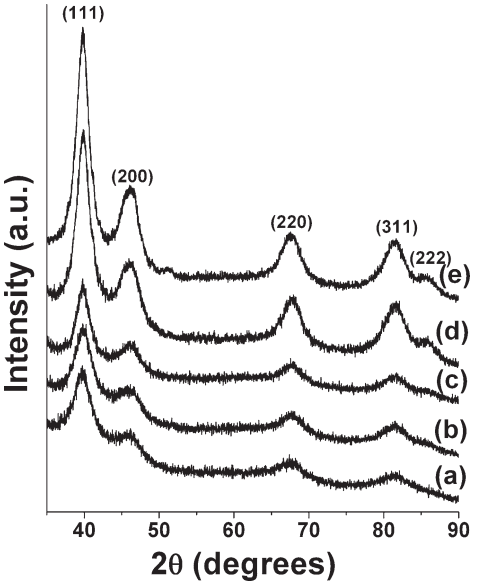

Figure 4. X-ray diffractograms of the platinum nanoparticles samples: (a) **PtNP-30**, (b) **PtNP-60**, (c) **PtNP-90**, (d) **PtNP-180**, and (e) **PtNP-300**.

modification to the synthetic procedure, characterized by an inversion of the sequence in which the dodecanethiol and the sodium borohydride are introduced to the solution. Instead of the original procedure, we would introduce the sodium borohydride solution before the dodecanethiol, aiming for the initial reduction of $[PtCl_6]^{2-}$ to Pt^0, followed by the introduction of dodecanethiol, which could then attach to the surface of the freshly formed nanoparticles. If successful, control of the nanoparticle size could be achieved by altering the time between the beginning of the reduction (introduction of the borohydride solution) and the dodecanethiol introduction, which corresponds to the time during which the reduction takes place and during which growth of the nanoparticles is occurring (i.e., the time before the interruption of the growing step, which would be caused by attachment of the thiol molecules to the nanoparticle surface). As this time period increases, so does the growth time of the nanoparticles, and therefore larger nanoparticles will form. Thus, we prepared samples with reduction times of 30, 60, 90, 180, and 300 s, according the description in the Experimental Section.

In all experiments, a dramatic color change of the organic phase (light yellow to black) was observed after the reduction step. Figure 4 presents the X-ray diffractograms of the samples, showing the occurrence of the characteristics peaks of fcc platinum in all samples (the peak descriptions are indicated in Figure 4). It is noticeable that the samples obtained from smaller reduction times (**PtNP-30**, **PtNP-60**, and **PtNP-90**) present broader peaks in the XRD profile (parts a, b, and c of Figure 4, respectively), indicating smaller particle size. The bandwidth of the XRD peaks should be qualitatively indicative of the particle size. Taking the (111) peak as a reference, the bandwidth became sharper with an increase in the reduction time, which is due to an increase in the particle size.

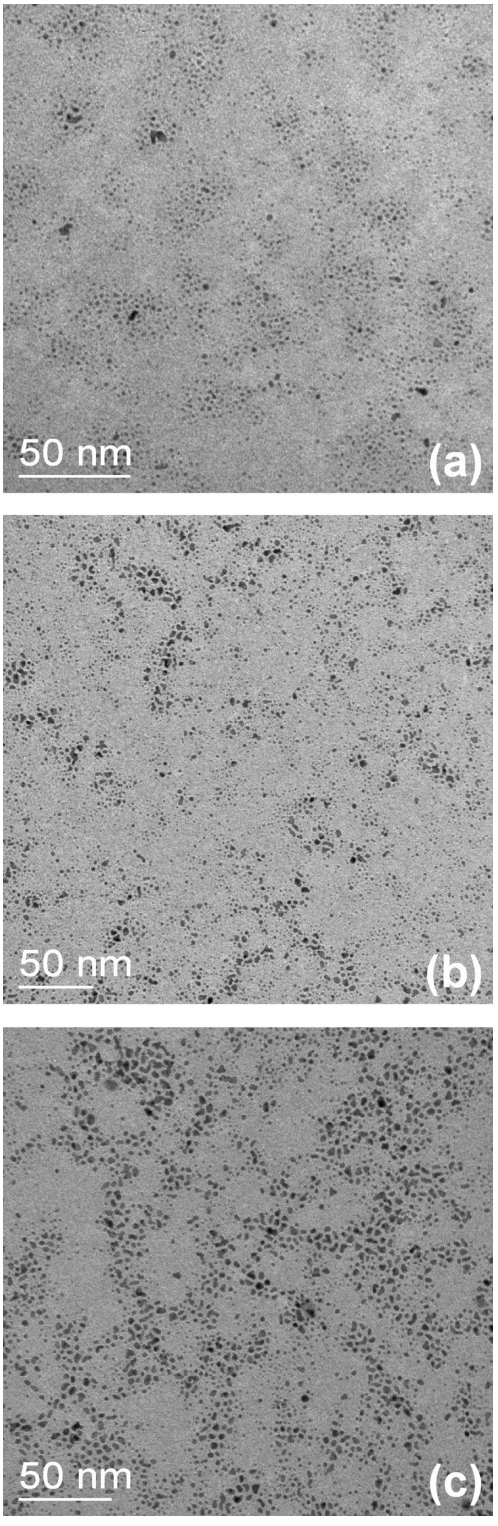

Figure 5. TEM images of the Pt nanoparticles samples: (a) **PtNP-30**, (b) **PtNP-60**, and (c) **PtNP-90**.

The sharp bandwidth observed in the XRD profile of the samples with reduction times of 180 s or longer (**PtNP-180** and **PtNP-300**) indicates that the particles are of larger size (as can be proved by the TEM image of the **PtNP-180** sample presented in Figure S8 in the Supporting Information). This fact is corroborated by the instability of the samples in toluene. Once the samples were synthesized, washed, and characterized,

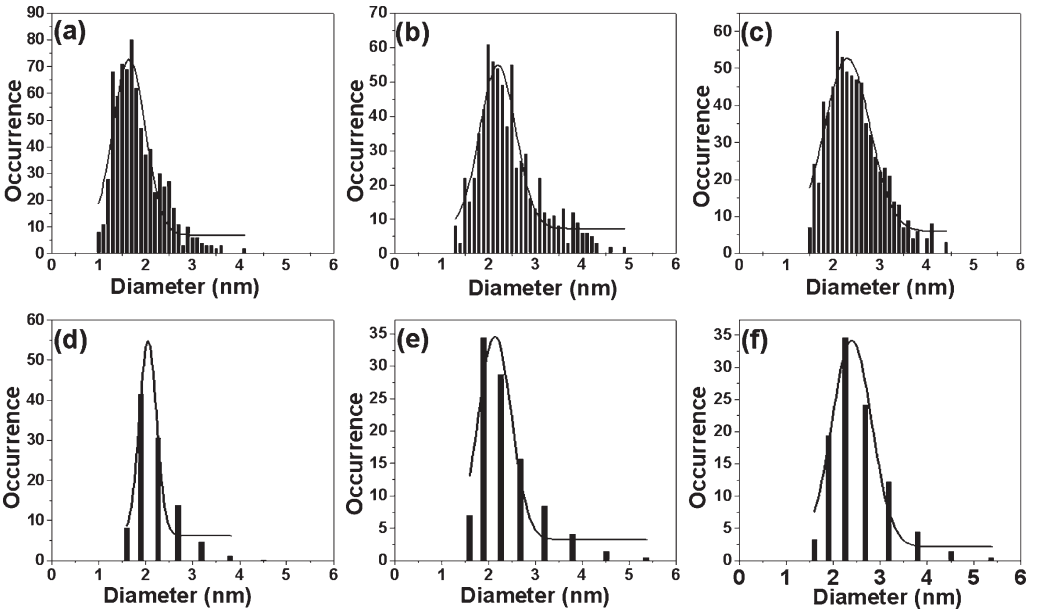

Figure 6. Size histograms estimated from the TEM images (a−c) and from DLS analysis of toluene dispersion (d−f) of the Pt nanoparticles samples: (a,d) **PtNP-30**, (b,e) **PtNP-60**, and (c,f) **PtNP-90**.

they were redispersed in toluene to assess their stability. We noted that the samples **PtNP-180** and **PtNP-300** did not disperse and instead precipitated. In contrast, samples **PtNP-30**, **PtNP-60**, and **PtNP-90** remained stable in toluene. The solutions were monitored for 1 month, and no degradation or precipitation was observed during this time. Because our interest is centered on the preparation of stable platinum nanoparticles, we decided to focus our studies only on the samples in which nanoscale particles were formed: **PtNP-30**, **PtNP-60**, and **PtNP-90**.

Figure 5 shows the transmission electron microscopy (TEM) images of **PtNP-30**, **PtNP-60**, and **PtNP-90**, and Figure 6 shows the size histograms estimated from the TEM image analysis of ~750 particles from each sample. Size histograms obtained by dynamic light scattering (DLS) from the toluene dispersions of the nanoparticles are also presented in Figure 6. The TEM images indicate very small and nonagglomerated nanoparticles for all three samples, with medium particle diameters of 1.7 ± 0.3, 2.2 ± 0.4, and 2.4 ± 0.5 nm for the samples **PtNP-30**, **PtNP-60**, and **PtNP-90**, respectively. The particle sizes estimated by the TEM data match well with the data obtained by DLS (2.0 ± 0.2, 2.2 ± 0.4, and 2.4 ± 0.4 nm for the samples **PtNP-30**, **PtNP-60**, and **PtNP-90**, respectively, Figure 6).

Figure 7 presents the HRTEM images of individual particles collected from samples **PtNP-30** (Figure 7a,b), **PtNP-60** (Figure 7c), and **PtNP-90** (Figure 7d,e). The high crystallinity of the particles is evidenced by the atomic arrangement or lattice fringes observed, which can be attributed to crystalline planes of fcc platinum. It is clear from the images shown in Figure 7 that the particles have characteristics of single crystals. Figure 8 show some selected images found in sample **PtNP-90**. Contrary to the majority of the particles observed in other samples, these images show structures with elongated shape, characterized by two or more nanoparticles connected through necks. These results are evidence of the

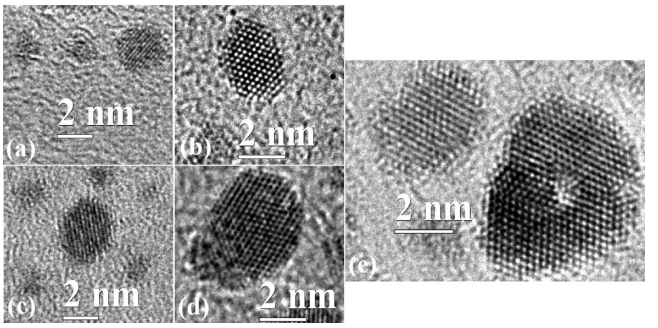

Figure 7. HRTEM images of the Pt nanoparticles samples: (a,b) **PtNP-30**, (c) **PtNP-60**, and (d,e) **PtNP-90**.

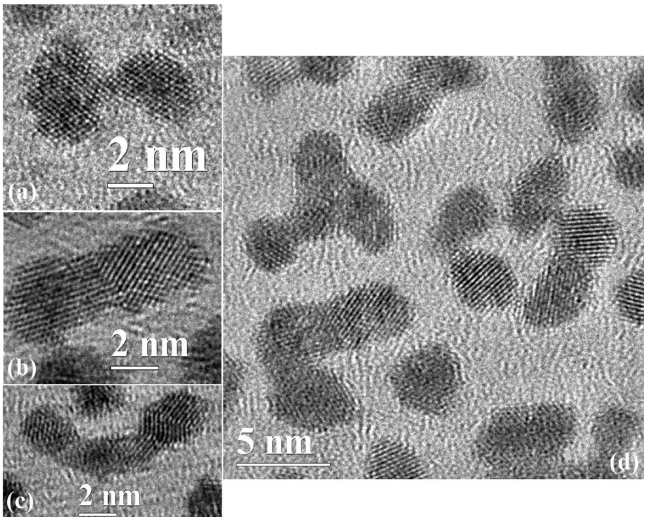

Figure 8. HRTEM images of the selected particles of the sample **PtNP-90**.

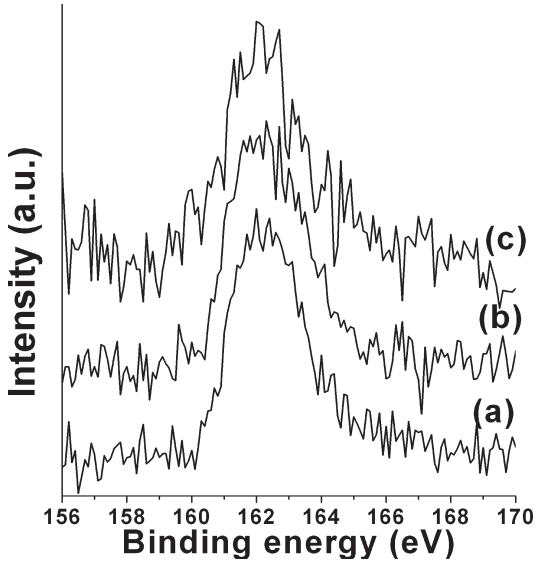

Figure 9. XPS spectra (S 2p region) of the Pt nanoparticles samples: (a) **PtNP-30**, (b) **PtNP-60**, and (c) **PtNP-90**.

beginning of the growing process in which two (or more) individual particles aggregate to initiate formation of a larger particle. The growing process was probably interrupted by the adsorption of dodecanethiol molecules onto the surface of the joining particles. At the start of the reaction several nuclei are formed, and each begins to grow. The growing is quickly interrupted in the sample **PtNP-30**, which results in nanoparticles with smaller diameters (Figures 6a and 7a,b). If the time before dodecanethiol addition is increased (as with sample **PtNP-90**), the unprotected nanoparticles have mobility in solution and can coalesce, until the moment at which the dodecanethiol is introduced in the system. The image in Figure 8a shows clearly two nanoparticles in the beginning of the coalescence. Figure 8b shows two bonded particles with shared crystalline faces, and Figure 8c shows an elongated particle formed by the aggregation of three primary nanoparticles. The images detailed in Figure 8b–d should be representative of structure intermediates between the beginning of the coalescence and the formation of larger particles.

The presence of dodecanethiol in the resulting platinum nanoparticles was confirmed by both FT-IR and XPS analysis. The infrared spectra of the nanoparticles show typical dodecanethiol bands (Figure S7 in the Supporting Information). The characteristic C–H stretching modes at 2960, 2929, 2877, and 2856 cm^{-1} in the nanoparticle samples are sharper than the same bands observed in the pure dodecanethiol spectrum, indicating restricted movements due to interactions between neighboring molecules adsorbed on the surface of the platinum NPs.[40]

The XPS spectra of the platinum nanoparticle samples prepared in this work are presented in Figures 9 (S_{2p} region) and 10 (Pt_{4f} region). The binding energy of S_{2p} for

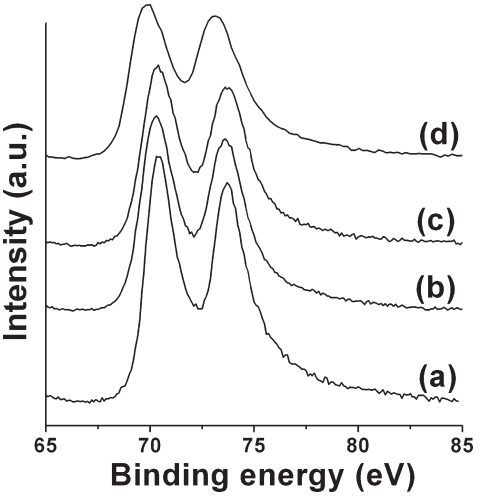

Figure 10. XPS spectra (Pt 4f region): (a) Pt foil, (b) **PtNP-30**, (c) **PtNP-60**, and (d) **PtNP-90**.

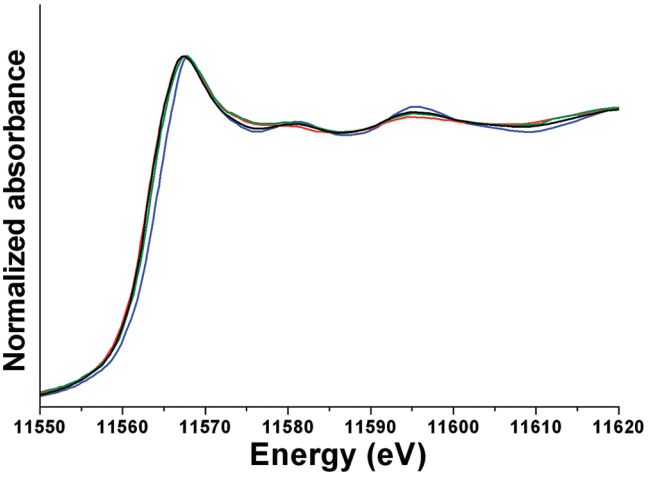

Figure 11. XANES spectra: Pt foil (blue), **PtNP-30** (red), **PtNP-60** (green), and **PtNP-90** (black).

the samples **PtNP-30**, **PtNP-60**, and **PtNP-90** was 162.1, 162.2, and 162.1 eV, respectively. These values shifted to a lower binding energy when compared to the pure dodecanethiol molecules (163.2 eV),[41] which has been attributed to a strong interaction between the sulfur atoms of the dodecanethiol molecules and the nanoparticle surface.[41,42] The XPS spectra in the Pt_{4f} region are shown in Figure 10. The two observable peaks are due to the $Pt_{4f7/2}$ and $Pt_{4f5/2}$ electrons, which have binding energies of 73.7 and 70.4 eV, respectively.[41,42] These binding energies are comparable to those of bulk platinum, confirming the zerovalent state of the platinum in the nanoparticle samples. The XPS peaks in the nanoparticle spectra are significantly broader than in the spectrum of bulk platinum (for the peak $Pt_{4f5/2}$ the fwhm = 2.4, 2.7, 2.8, and 3.3 eV for the samples Pt-bulk, **PtNP-30**, **PtNP-60**, and **PtNP-90**, respectively. For the

(40) Badia, A.; Cuccia, L.; Demers, L.; Morin, F.; Lennox, R. B. *J. Am. Chem. Soc.* **1997**, *119*, 2682.

(41) Tu, W. X.; Takai, K.; Fukui, K.; Miyazaki, A.; Enoki, T. *J. Phys. Chem. B* **2003**, *107*, 10134.

(42) Fu, X. Y.; Wang, Y.; Wu, N. Z.; Gui, L. L.; Tang, Y. Q. *J. Colloid Interface Sci.* **2001**, *243*, 326.

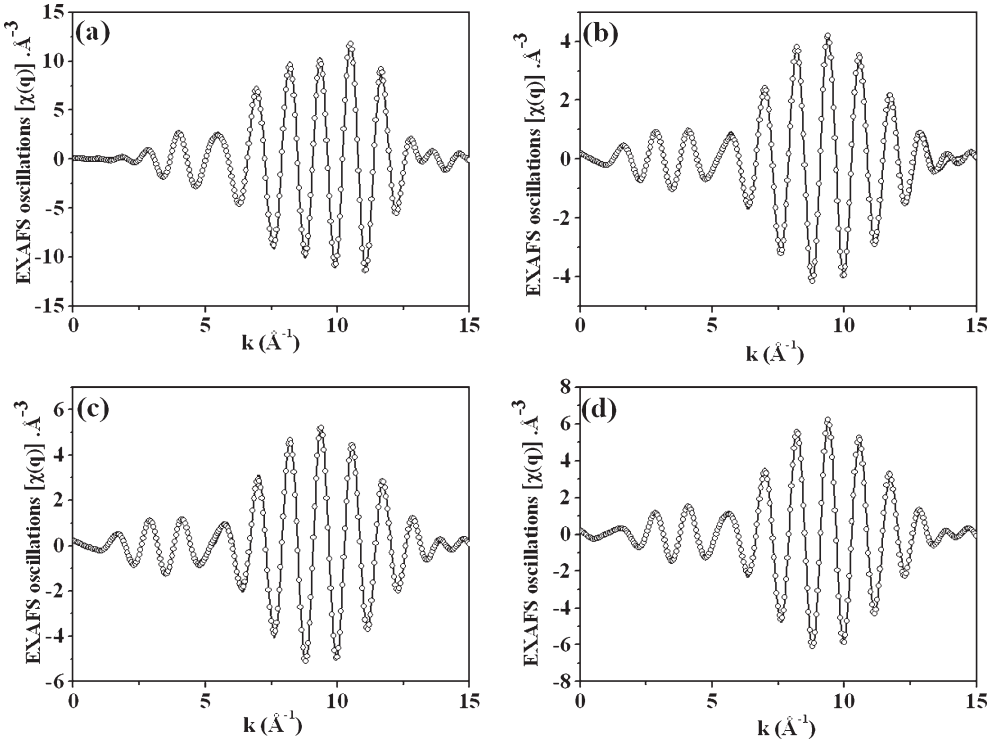

Figure 12. Experimental (continuous line) and fitted (dotted line) Pt L_3-edge EXAFS spectra: (a) Pt foil, (b) **PtNP-30**, (c) **PtNP-60**, and (d) **PtNP-90**.

peak $Pt_{4f7/2}$, the fwhm = 1.9, 2.3, 2.5, and 2.8 for the same samples, respectively). This broadening is likely related to the contribution of surface platinum atoms that are directly linked to the dodecanethiol molecules, which should present lower electronic density in comparison to the platinum atoms not at the surface.[17]

The nanoparticle samples were also characterized by XAS. The XANES spectra of the samples are shown in Figure 11. The intensities of the white lines in the spectra of all nanoparticle samples and of bulk platinum are comparable, corroborating the previous data that the nanoparticles in **PtNP-30**, **PtNP-60**, and **PtNP-90** consist of zerovalent platinum.

The experimental EXAFS spectra of the nanoparticle samples were fitted (Figure 12) and Fourier transformed (Figure 13). The FTs show an intense peak between 2 and 3 Å, corresponding to a Pt−Pt scattering path related to the first coordination shell around the absorber. The amplitude of this peak is highest for bulk platinum and is strongly reduced for the nanoparticle samples. The amplitude decreases gradually from sample **PtNP-90** to **PtNP-60** to **PtNP-30**, and this decrease is caused by the reduction in the average Pt coordination number, which is associated with the large number of surface atoms in

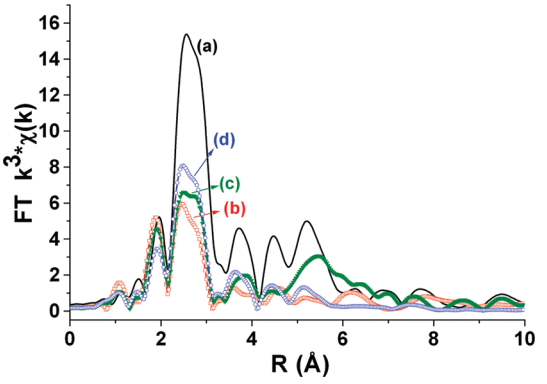

Figure 13. Fourier transformed EXAFS spectra: (a) Pt foil, (b) **PtNP-30**, (c) **PtNP-60**, and (d) **PtNP-90**.

very small particles.[43−47] As the particle gets smaller, the ratio of surface-to-bulk atoms increases and the average coordination number is expected to be lower. The coordination number obtained by the EXAFS data decreases gradually from sample **PtNP-90** to **PtNP-60** to **PtNP-30** (Table 1), following the nanoparticle size trend. A slight contraction in the Pt−Pt bond lengths was also observed in the nanoparticle samples (related to the bulk platinum, Table 1), and this effect has been correlated with a contraction of the lattice due a higher energy surface caused by incomplete coordination of the atoms at the surface.[43−47] This effect was followed by an increase in the Debye−Waller factor (proportional to the decrease in particle size) indicating a small disorder in the lattice according to the reduction in the particle size, as expected.

The catalytic performance of metal nanoparticles is dependent on several factors such as size, morphology,

(43) Frenkel, A. I.; Hills, C. W.; Nuzzo, R. G. *J. Phys. Chem. B* **2001**, *105*, 12659.
(44) Calvin, S.; Luo, S. L.; Caragianis-Broadbridge, C.; McGuinness, J. K.; Anderson, E.; Lehman, A.; Wee, K. H.; Morrison, S. A.; Hurihara, L. K. *Appl. Phys. Lett.* **2005**, *87*, 233102.
(45) Roman-Martinez, M. C.; Macia-Agullo, J. A.; Vilella, I. M. J.; Cazorla-Amoros, D.; Yamashita, H. *J. Phys. Chem. C* **2007**, *111*, 4710.
(46) Shih, C.-C.; Chang, J.-R. *Mater. Chem. Phys.* **2005**, *92*, 89.
(47) Zhang, Y.; Toebes, M. L.; van der Eerden, A.; O'Grady, W. E.; Jong, K. P.; Koningsberger, D. C. *J. Phys. Chem. B* **2004**, *108*, 18509.

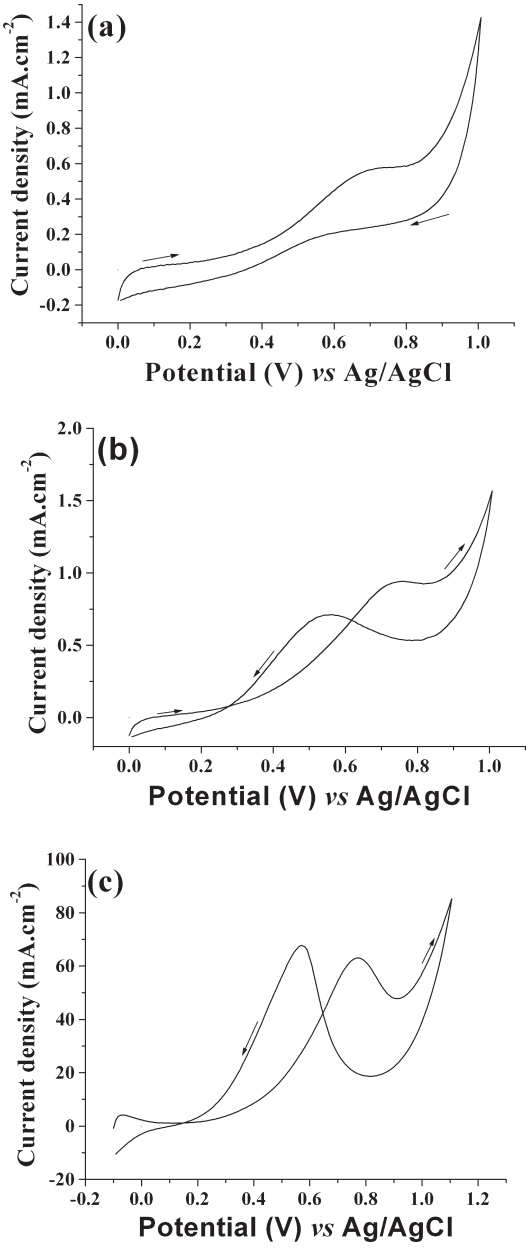

Figure 14. Current−potential curves for methanol oxidation reaction on (a) **PtNP-30** (b) **PtNP-60**, and (c) **PtNP-90**, in 1 mol L^{-1} CH_3OH + 0.5 mol L^{-1} H_2SO_4 at room temperature. Scan rate = 50 mV s^{-1}.

purity, and type of stabilizer in their surface. The influence of the type of stabilizer molecules on the catalytic effectiveness has been recently demonstrated by Yang et al.[13] These authors showed that divergence in the binding affinities of dodecanethiol and dodecylamine for Pt nanoparticles with different sizes results in differences in the catalytic activities of these materials. To verify the electrocatalytic activity of our nanoparticle samples, we carried out cyclic voltammetry measurements on a methanol solution (1 mol L^{-1} CH_3OH in 0.5 mol L^{-1} H_2SO_4 at room temperature), employing working electrodes based on the NP samples (see the Experimental Section). The results are shown in Figure 14. The voltammograms are characteristic and show a forward (anodic) peak due to methanol oxidation and a back (anodic reverse) peak attributed to removal of the incompletely oxidized carbonaceous species formed in the forward scan.[5,13,48−50] The peak current densities of the forward peak can be used to evaluate the catalytic activity. The **PtNP-90** shows the highest catalytic activity and a high current density (63 mA cm^{-2}), comparable to the best results present in the literature.[5,13,48−50] The current density of this sample was higher than that of **PtNP-60** by 63 times (current density = 1 mA cm^{-2} for the sample **PtNP-60**). Since the size of these particles is comparable (2.2 and 2.4 nm), the explanation for these differences should be related to both the poor covering of the NPs surface by the thiol molecules in **PtNP-90**, which means more catalytic sites available in this sample (the S/Pt molar ratio obtained by XPS was 1.67 to **PtNP-90** and 2.77 to **PtNP-60**, evidencing the poorest covering of the former) and the occurrence of the nanoparticles in the beginning of the coalescence process in **PtNP-90** (discussed in the HRTEM images), which probably have more unprotected surface area available for catalytic activity. In contrary, the very poor catalytic activity exhibited by **PtNP-30** (current density = 0.7 mA cm^{-2}) should be related to the small size of the particles. The surface of the nanoparticles is probably fully covered by thiol molecules, which makes the approach of methanol molecules difficult due to steric effects.

Conclusions

A successful route for the preparation of dodecanethiol-stabilized platinum nanoparticles through a two-phase liquid−liquid route was described. The occurrence of a stable complex between the platinum precursor and the dodecanethiol molecules was demonstrated for the first time, and previous unsuccessful attempts to prepare Pt NPs by this route were attributed to the stability of this complex to borohydride reduction. A simple inversion in the sequence of reagent additions was proposed, resulting in an efficient route for preparing stable and very small Pt nanoparticles. The electrocatalytic activity of the nanoparticles was tested in methanol oxidation, and the results indicate very good performance for the sample **PtNP-90**. We believe that the electrocatalytic properties of the NPs produced here can be improved by the deposition of these particles on suitable carbonaceous materials and by further studies on the construction of electrodes. Efforts in these directions are underway in our laboratory.

Acknowledgment. The authors acknowledge the financial support from CNPq, CAPES/PROCAD, Brazilian Network on Carbon Nanotubes Research (MCT/CNPq), and INCT-Nanocarbono (MCT/CNPq). We also acknowledge CME-UFPR for the TEM images and LNLS−National Synchrotron Light Laboratory, Brazil (Project HRTEM 6777 and XAS) for the HRTEM images and XAS data. E.G.C. and R.V.S. acknowledge CAPES for fellowships.

(48) Sun, C.-L.; Chen, L.-C.; Su, M.-C.; Hong, L.-S.; Chyan, O.; Hsu, C.-Y.; Chen, K.-H.; Chang, T.-F.; Chang, L. *Chem. Mater.* **2005**, *17*, 3749.
(49) Lima, F. H. B.; Gonzalez, E. R. *Electrochim. Acta* **2008**, *53*, 2963.
(50) Kim, Y.-T.; Mitani, T. *J. Catal.* **2006**, *238*, 394.

Supporting Information Available: UV−vis spectra of the aqueous solution of H_2PtCl_6; XANES spectra of the aqueous solution of H_2PtCl_6, showing the A and B peaks weights used in determining the ratio A/B; proposal mechanism and optimized structures for the formation of complexes **Pt/DT-1/2** and **PT/DT-1/4**; FTIR spectra of the nanoparticles; and TEM image of the **PtNP-180** sample (PDF). This material is available free of charge via the Internet at http://pubs.acs.org.